

Paleozoic xenoliths in Eocene plutons: The evidence for the destruction of pre-Jurassic crystalline basement beneath Adjara–Trialeti belt, Lesser Caucasus

AVTANDIL OKROSTSVARIDZE^{1,✉}, YU-HAN CHANG², SUN-LIN CHUNG^{2,3},
FABIEN RABAYROL⁴, GIORGI BOICHENKO¹ and SALOME GOGOLADZE¹

¹Institute of Earth Sciences, Ilia State University, Tbilisi, Georgia; ✉okrostsvari@gmail.com

²Department of Geosciences, National Taiwan University, Taipei, Taiwan

³Institute of Earth Sciences, Academia Sinica, Taipei, Taiwan

⁴MDRU-Mineral Deposit Research Unit, the University of British Columbia, Vancouver, Canada

(Manuscript received December 22, 2020; accepted in revised form June 16, 2021; Associate Editor: Igor Broska)

Abstract: In Georgia the Paleogene Adjara–Trialeti riftogenic belt (length 350 km, width 50–2 km) is dominantly composed of trachytic and trachytic–andesitic pyroclastic deposits, though plutonic rocks also play an important role in the structure. In this article, we report new data on the (LA-ICP-MS) U–Pb zircon geochronology and petrochemistry of the plutons, their xenoliths and restite from this belt. The results indicate that the magmatism in the basin began in the Early Eocene (~50 Ma) associated with the formation of pyroclastic rocks. The mafic intrusions (~46–44 Ma) led to the assimilation and contamination of sialic crust and formation of monzo-syenite melts emplaced at ~43–42 Ma. The Eocene monzo-syenite plutons contain xenoliths of Paleozoic granites (312±7 to 474±5 Ma) and tholeiitic basalts that contain inherited zircon grains ranging in age from Neo-Proterozoic (747±33 Ma, 632±29 Ma) to Cambrian (515±9 Ma). Paleozoic granite xenoliths show complete mineralogical and age similarity to the Adjara–Trialeti belt adjacent pre-Jurassic massif granites. Inherited zircon grains most likely are captured by magmas during ascent that cuts through the Gondwana-derived old continental crust. Obtained results and regional geological analysis demonstrate that the riftogenic basin of the Adjara–Trialeti belt developed on the pre-Jurassic crystalline basement, from Late Cretaceous to Eocene into a back-arc extensional regime to post-collision geodynamic setting.

Keywords: Adjara–Trialeti belt, plutons, xenolith, zircon U–Pb geochronology.

Introduction

From the Late Cretaceous to the Eocene, the Adjara–Trialeti fold-thrust belt with a length of more than 350 km is clearly expressed from the east of Tbilisi to the west to the Black Sea. It was interpreted as a back-arc rift that formed in the north of the Mesozoic island arc of the Lesser Caucasus (Gamkrelidze 1974, 1986; Lordkipanidze et al. 1979; Lordkipanidze 1980). Timing of the Adjara–Trialeti volcano-sedimentary sequence was initially constrained by paleontology (Laliev & Zirakadze 1971) and subsequently, by laser ablation ICP-MS U–Pb geochronology of the plutonic rocks zircons (Okrostsvaridze et al. 2018).

Igneous rocks of the Adjara–Trialeti belt are dominated by monzo-syenite plutons and trachytes, which are believed to have formed either as a result of arc subduction (Duggen et al. 2005), mantle plume activity (DePaolo & Managa 2003; Ashwal et al. 2016), post-collisional tectonic setting (Chung et al. 2005; Keskin et al. 2006), or continental rifting (Peccerillo et al. 2003). Despite these contradictory views, it is recognized in all cases that magmatism suggests the influence of mantle flows on the crust and subsequent processes of assimilation and contamination.

Field evidence indicates that these Middle Eocene monzo-syenite plutons contain numerous xenoliths of granites and basalts, as well gabbroid restites. Despite the fact that there are time constraints for these Eocene plutons, the age and implications for the xenoliths and restites have not been discussed before in the context of regional magmatic and geodynamic evolution of crystalline basement beneath this Adjara–Trialeti belt.

In this context, xenoliths and restites provide important information about the source and geodynamic setting for the formation of felsic melts (Didier 1973; Didier & Barbarin 1991; Barbarin 2005; Shellnutt et al. 2010; Zhao et al. 2012) and assimilation processes between crustal- and mantle-derived magmas (Griffin et al. 2002; Liu et al. 2013; Yu et al. 2018).

We believe that Late Cretaceous–Eocene Adjara–Trialeti belt provides a suitable area for the investigation of extensional and magmatic processes, and the underlying structure of the Lesser Caucasus. Based on information obtained from the enclaves, we set the main goal of our research – to find out the type and age of the basement. To solve this problem we present here new LA-ICP-MS U–Pb zircon geochronological and petrochemical data on the plutons and their xenoliths and

restites along the Adjara–Trialeti belt. We define the geochemical signatures of Eocene plutons, constrain their timing and investigate their magmatic processes and tectonic affinity in the context of a collisional setting.

Geological background of the region

The Paleogene Adjara–Trialeti riftogenic basin is located in the 1200 km-long Caucasus orogenic belt, between the Caspian and Black seas (Fig. 1). This belt resulted from the successive collisions and accretions of the Gondwana-derived Rhodope–Pontide, Anatolia and Arabia crustal blocks to the Scythian platform of the Eurasian continent during the closure of the Paleo-Tethys and Neo-Tethys oceans since the Paleozoic (e.g., Sengor & Yilmaz 1981; Gamkrelidze 1986; Stampfli & Borel 2004; Richards 2015; Rabayrol et al. 2019).

The Greater Caucasus fold-and-thrust belt is the northernmost expression of the Caucasus orogen and is linked to the southern margin of the Eurasian continent. It developed during the Late Proterozoic, Paleozoic and Mesozoic as a result

of north-dipping subduction of the Paleo-Tethys beneath the Scythian platform (Zaridze & Shengelia 1978; Gamkrelidze 1986; Okrostsvaridze 2007; Somin 2011; Okrostsvaridze & Tormay 2013; Gamkrelidze et al. 2020). The crystalline basement of the Caucasus (200 km length and 20–30 km width) was affected by the pre-Variscan and Variscan orogenies that produced Precambrian and Paleozoic crystalline schists, amphibolites, ophiolites, gneisses, migmatites and granitoids (Gamkrelidze & Shengelia 2005; Okrostsvaridze & Tormay 2011; Gamkrelidze et al. 2020).

The Mesozoic and Cenozoic volcano-sedimentary sequences of the Caucasus are mainly composed of Lower Jurassic black-schist, Bajocian volcanic rocks and Lower Cretaceous carbonate rocks. This volcano-sedimentary sequence was intruded by Middle Jurassic plutons (Dudauri & Togonidze 2016).

The Greater Caucasus is bordered to the south by the Transcaucasus microplate, which comprises Meso–Cenozoic sediments and Gondwana-derived crystalline massifs (Zakariadze et al. 2007; Okrostsvaridze & Tormay 2013; Okay & Topuz 2017). South of the Transcaucasian microplate, the Lesser Caucasus unit records the Mesozoic subduction of the Northern

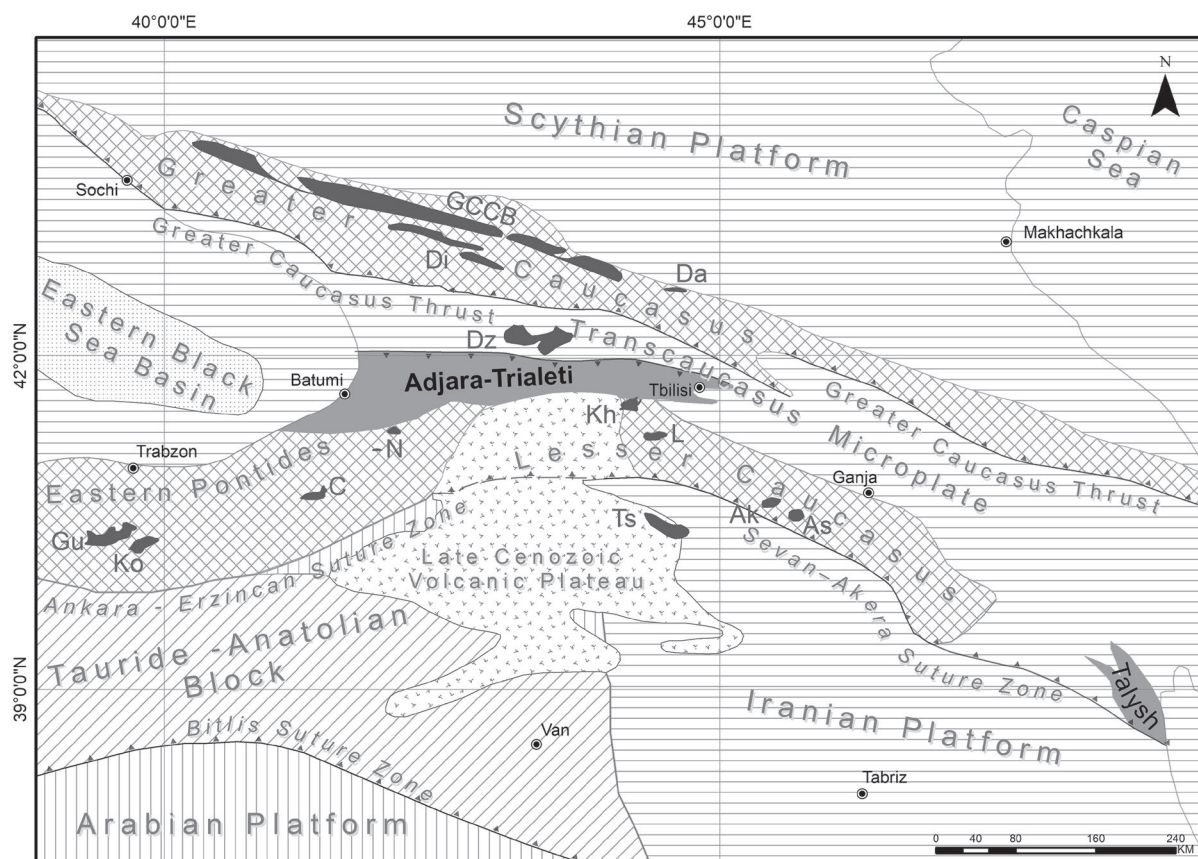


Fig. 1. Simplified schematic geological map of the Arabian–Eurasian collision segment of the Alpine–Himalayan orogenic belt. Pre-Jurassic outcrops: GCCB – Greater Caucasus crystalline basement, Da – Dariali massif, Di – Dizi series, Dz – Dzirula massif, Kh – Khrami massif, L – Loki massif, Ak – Akhum massif, As – Asrikchai massif, Ts – Tsakhuniats massif, N – Nartic massif, C – Camukaua massif, Ko – Kose massif, Gu – Gumushane massif (adapted after Philip et al. 1989; Yilmaz et al. 2000; Gamkrelidze 2003; Moritz et al. 2016, Okay & Topuz 2017).

Neo-Tethyan oceanic crust and subsequent collision with the Rhodope–Pontide, Anatolide–Tauride and South Armenian blocks along the Late Cretaceous Izmir–Ankara–Erzincan and Sevan–Akera suture zones (Gamkrelidze 1986; Zonenshain & Le Pichon 1986; Philip et al. 1989; Rolland et al. 2012).

The Lesser Caucasus is divided into four tectonic zones from north to south: 1) The Artvin–Bolnisi zone consists of the Cretaceous units in the northern part of the Somkheto–Karabagh belt, south of the Transcaucasus (Gamkrelidze 1986; Yilmaz et al. 2000); 2) The magmatic and sedimentary units of the Somkheto–Karabagh arc belt and the Kapan zone that was the active margin of Laurasia during the Mesozoic; 3) The obducted ophiolitic melange of the Sevan–Akera suture zone that represents the remnants of the Neotethys oceanic crust; 4) The Gondwana-derived South Armenian block (Sosson et al. 2010; Mederer et al. 2013).

The easternmost segment of the Lesser Caucasus is represented by the Talysh Rift Zone near the Caspian Sea (Fig. 1), which was formed during the extension of the Transcaucasus microplate from Late Cretaceous to Eocene, similarly to the Adjara–Trialeti riftogenic basin. The Talysh Rift Zone is characterized by volcanoclastic basaltic rocks, tuff turbidites and terrigenous material and extends eastwards under the Caspian Sea (Vincent et al. 2005).

Pre-Jurassic crystalline basement outcrops of the region

Pre-Jurassic crystalline basement outcrops occupy a small area in the study region (Fig. 1). The basement is exposed in the Greater Caucasus in the following zones: the Fore Range, Main Range and Southern Slope. Through the Transcaucasus microplate the pre-Jurassic basement outcrops in the Dzirula and Khrami massifs, while in the Lesser Caucasus it is exposed as the Loki, Akhum and Asrikchai massifs (Gamkrelidze & Shengelia 2005). In the South Armenian Block Pre-Jurassic basement crops out as the Tsakhuniats massif (Agamalian 2004). We will briefly describe here only those massifs, which border the North and South of the Adjara–Trialeti belt.

The Dzirula crystalline massif (~1200 km²) which crops out to the north of the Adjara–Trialeti belt is mainly made of Neoproterozoic plagiomigmatites, crystalline schists, and ophiolites; Lower Paleozoic biotite granodiorite gneisses and Upper Paleozoic anatectic microcline-bearing granites. The Rb–Sr age data yield 686±74 Ma for plagiomigmatites, whereas 331±21 Ma for microcline granites (Okrostsvaridze & Clarke 2004). The same microcline granites were dated by Lu–Hf geochronology and the obtained data vary between 322 and 309 Ma (Chiu et al. 2015). The Neoproterozoic ophiolite units in the north-eastern part of the Dzirula massif define the Chorchana–Utslevi Ophiolitic Zone (Gamkrelidze et al. 1981). Those ophiolites come into contact with the gneiss-migmatite complex and are cut by the Upper Paleozoic microcline granites.

The Khrami crystalline massif crops out to the south of the Adjara–Trialeti belt and represents a large (~500 km²) uplifted part of the Artvin–Bolnisi block. It is mainly composed of the pre-Variscan migmatite-gneiss complexes and the Upper Variscan granites that crystallized at 333±20 Ma (LA-ICP-MS U–Pb dating on zircon (Gamkrelidze & Shengelia 2005)).

The pre-Jurassic basement of the region extends to the west on the Rhodope–Pontide block and includes the Natric, Camukaua, Kose and Gumushane massifs (Topuz et al. 2010; Okay & Topuz 2017). Carboniferous granites of these massifs intruded into the LP–HT metamorphic rocks and are unconformably overlain by Lower Jurassic continental to marine sandstones (Topuz et al. 2010). These massifs are characterized by the similar petrography and petrochemistry, as well as isotopic geochronology. The LA-ICP-MS zircon U–Pb ages of the Upper Paleozoic granites vary between 330 and 294 Ma (Topuz et al. 2010).

Adjara–Trialeti belt

The Adjara–Trialeti belt spreads out from Tbilisi (the Iori River gorge) toward the Black Sea in the west. The length of the belt is ~350 km in the eastern part, gradually increasing in width westwards from 2 km to 50 km in the Black Sea area (Fig. 1). This volcano-sedimentary basin formed on the Lesser Caucasus basement and got inverted in the Oligo–Miocene to form a fold-and-thrust belt (Gamkrelidze 1974).

The volcano-sedimentary sequence of the Adjara–Trialeti belt was thrust over the Transcaucasus microplate to the north. The southern border of the Adjara–Trialeti belt is covered by the Upper Cenozoic, thick, sub-aerial pyroclastic material and lava flows.

Gamkrelidze (1976) suggests the Adjara–Trialeti rift was formed on the south-eastern edge of the Transcaucasus microplate. This microplate, during the late Carboniferous, was the accumulation area of shallow marine and volcanic deposits. During the Early Jurassic epoch, thin layers of clay-sandy and carbonate composition were deposited. From the Middle Jurassic to Early Cretaceous the massif was exhumed and eroded (Gamkrelidze 1986).

From the Early Cretaceous, especially during the Albian and Cenomanian times, the rifting processes started throughout the massif. The Transcaucasus microplate was gradually separated from the blocks of the southern province, which are called the Artvin–Bolnisi and Loki–Karabagi massifs in the modern structure of the Caucasus (Gamkrelidze 1986).

In the beginning of Paleogene, the rift already existed between the Transcaucasus and Artvin–Bolnisi massifs, that was also the area of intensive deposition. During the Paleocene–Early Eocene mostly terrigenous-carbonate materials were deposited, followed by volcanic rocks in the Middle Eocene (Gamkrelidze 1976). However, the type and rate of deposition was different in various segments of the Adjara–Trialeti belt. For instance, in the eastern part (modern Trialeti ridge) tuffs

and shales were deposited in the Middle Eocene, with the thickness of the deposits reaching on average 4–5 km. In the central part (modern Meskheti ridge), the volcanic rocks and the thickness of the units increases up to 5–6 km. In the western part of this massif in the Guria and Adjara mountains, extensive volcanic activity has produced volcanic deposits up to 7–8 km in thickness (Gamkrelidze 1976).

The seismic data in the western part of the Adjara–Trialeti belt, toward the Black Sea, indicates that the crust thins gradually (Balavadze et al. 1966). The thickness of the granitic layer gradually decreases and finally disappears in the central part of the Black Sea floor. Here the thickness of the basaltic layer decreases up to 5 km and it is overlain by deposits of 10–15 km in thickness (Balavadze et al. 1966).

The geodynamic evolution of the Adjara–Trialeti belt is controversial. One view suggests that its basin was formed in a back-arc setting based on analogous structures (e.g., the Talysh belt and Albors belt) in Iran (Gamkrelidze 1974; Vincent et al. 2005; Ballato et al. 2011; Asiabanha & Foden 2012). An alternative view argues for a post-collisional geodynamic setting for the Eocene magmatism of the Lesser Caucasus (Dilek et al. 2010; Sosson et al. 2010; Moritz et al. 2016). This interpretation is based on the age of continental collision between the Rhodope–Pontide block, on which the Transcaucasus massif is located, and the Anatolide–Tauride and South Armenian Blocks. The collision has been suggested to have occurred either in the Paleocene–Early Eocene (Yilmaz et al. 1997; Topuz et al. 2011; Robertson et al. 2013) or Late Cretaceous (Rolland et al. 2012; Meijers et al. 2015), before the formation of the Eocene Adjara–Trialeti belt (Fig. 2).

Adjara–Trialeti plutonism

Several plutons of different sizes are exposed in the Adjara–Trialeti belt. From West to East, they are the Namonastrevi, Merisi, Vakijvari, Zoti, Okrosgheli, Ghaghvi, Zekari, Rkviana and Khachkovi plutons, respectively. The plutonic bodies cover about 7 % of the surface area of the belt, but dominantly crop out in the western part of the belt, where their maximum extent was found (Fig. 3).

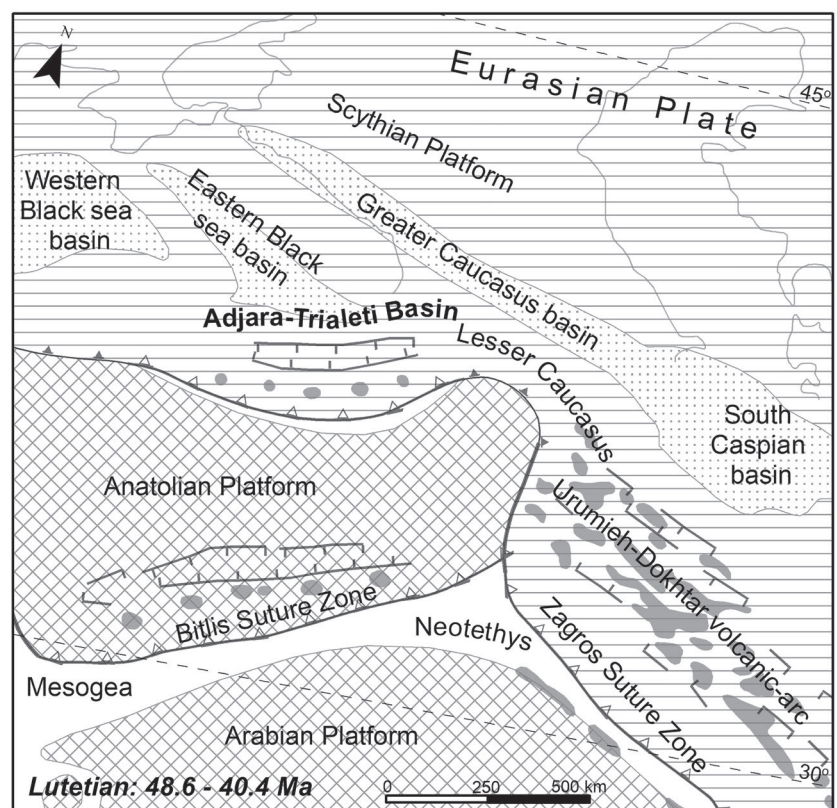
The plutons of the Adjara–Trialeti belt are dominantly composed of syenites and monzonites, but minor gabbroic, gabbro-and monzo-dioritic phases are also observed. Their mineral composition includes potassium feldspar, plagioclase feldspars, pyroxene, hornblende, biotite and magnetite

with accessory apatite, sphene and zircon. In the next paragraphs we will briefly describe only those plutons, which were dated.

The Merisi pluton (~10 km²) has an ellipsoidal shape and was intruded into the middle Eocene andesitic lavas and intermediate volcanoclastic deposits. It is dominantly consisting of a fine-grained, equigranular, hypidiomorphic, syenites and monzonites.

The Namonastrevi pluton (~7 km²), 2.5 km south-west of the Merisi pluton, is also intruded into the middle Eocene andesitic lavas and intermediate volcanoclastic deposits. The pluton is mainly composed of fine-grained, equigranular, hypidiomorphic, biotite monzonite.

To the north of the Namonastrevi pluton, the Vakijvari medium-grained, hypidiomorphic plutonic complex crops out. The complex is composed of the Bzhuzha (~3 km²), Vakijvari (~15 km²) and Korisbude unites (~2 km²), which are intruded into the middle Eocene intermediate tuff units. These units consist predominantly of syenites but minor gabbroic and monzonitic phases are also observed.



Legend

- | | |
|--|---|
| — Present day outline of the Black Sea and the Caspian Sea | ▣ Arabian plate and terranes of Gondwana origin |
| ▲ Active subduction zone | ▤ Eurasian Plate |
| ▲ Major thrust fault | ▥ Major basins |
| — Major strike-slip fault | ▧ Oceanic lithosphere |
| — Major normal fault | ■ Magmatism |

Fig. 2. Geodynamic reconstruction of the Central Tethyan region for Lutetian (48.6–40.4 Ma) (according to Moritz et al. 2016, simplified).

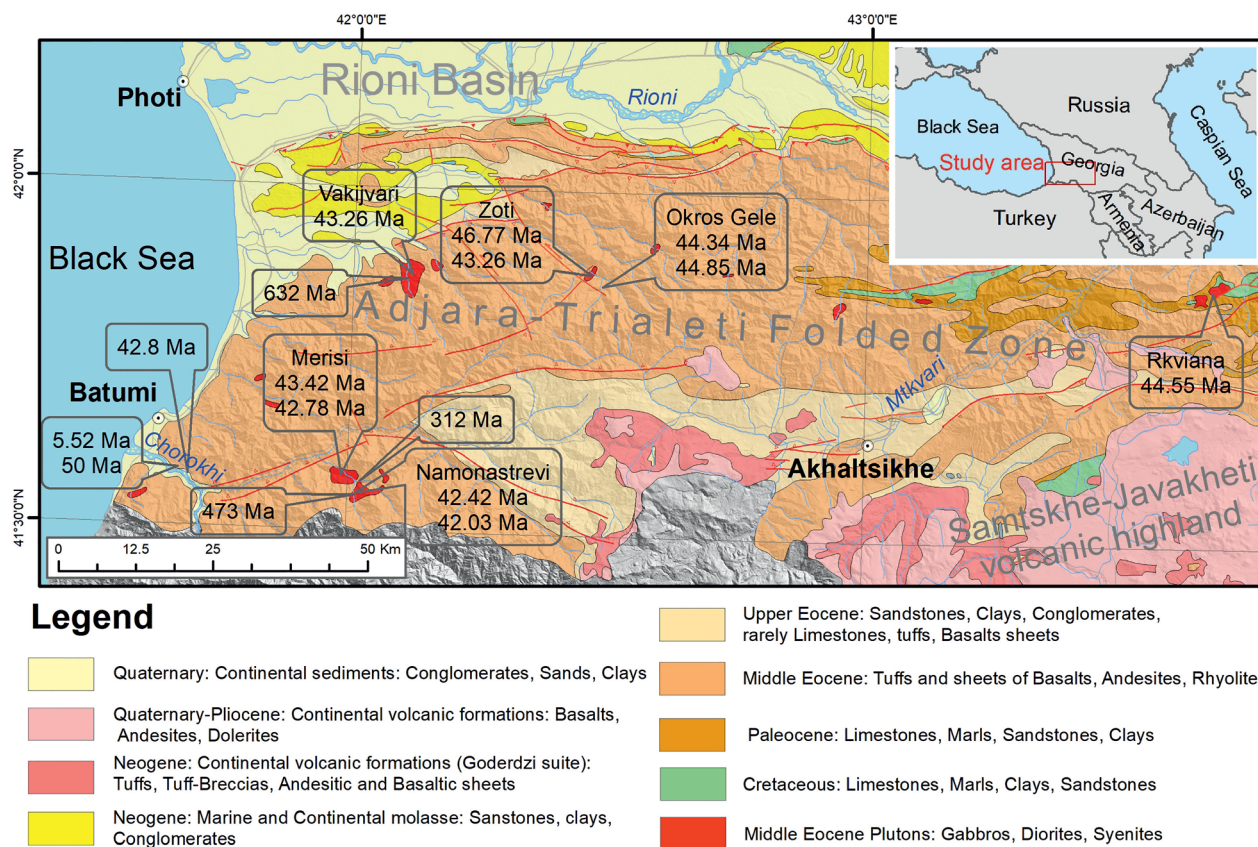


Fig. 3. Geological map with zircons U–Pb geochronological data of the plutons and their enclaves of the Adjara–Trialeti belt. It is adapted from Geological map of Georgia (Gamkrelidze 2003).

East of the Vakijvari pluton the Zoti pluton (~4.5 km²) crops out. It is intruded into the middle Eocene andesitic lavas and intermediate volcanoclastic deposits. It comprises mainly monzo-diorites but syenite and monzonite phases are also found.

Approximately 3 km south-west of the Zoti pluton, the Okros Gele (~1.5 km²) pluton crops out. It is composed of massive, medium-grained biotite-bearing syenites.

The Rkviana plutonic complex outcrops approximately 200 km to the east of the described plutons. This complex is composed of the Rkviana (~4 km²) and Gharta (~3 km²) units, which are intruded into the Upper Cretaceous limestones and the Lower-Middle Eocene intermediate tuff and sandstone successions. They consist of hornblende-rich, porphyritic diorite and hornblende–clinopyroxene-bearing, porphyritic gabbro.

Enclaves of the Eocene plutons

As mentioned in the introduction, xenoliths and restites provide important information about the source for the formation of felsic melts and assimilation processes between crustal and mantle-derived magmas. Due to the complexity of the topic, there are many interpretations of them (Didier & Barbarin

1991; Griffin et al. 2002; Barbarin 2005; Shellnutt et al. 2010; Zhao et al. 2012; Liu et al. 2013). In this publication, under the term “enclaves” we combine both xenoliths and restites. The remnants of the basic injections, which led to interaction between crustal- and mantle-derived magmas, are regarded as restites here.

The middle Eocene plutons of the Adjara–Trialeti belt contain numerous xenoliths, restites and mafic microgranular enclaves (Fig. 4).

The Namonastrevi pluton contains oval-shaped xenoliths of massive, medium-grained, light-coloured two-mica granite. Their main mineralogy consists of: microcline (30 %), plagioclase (27 %), quartz (25 %), biotite (7 %) and muscovite (5 %). Apatite, allanite, zircon and ore sulphide minerals occur as accessory minerals. The diameter of xenoliths varies from 20 to 120 cm; the xenolith volume can reach up to ~7 % of whole outcrops (Fig. 3). In the same intrusion, dark grey hornblende-biotite granodiorite xenoliths crop out. They also have an oval shape, but their size varies between 10–50 cm.

In the western periphery of the Vakijvari pluton numerous outcrops of oval-shaped basalt xenoliths are exposed (see Fig. 4D). The average sizes of the xenoliths is ~0.4 m × ~0.5 m.

These rocks are composed of plagioclase (up to 60 %), olivine (up to 5 %), augite (up to 20 %), epidote (up to 3 %) and volcanic glass (up to 10 %).

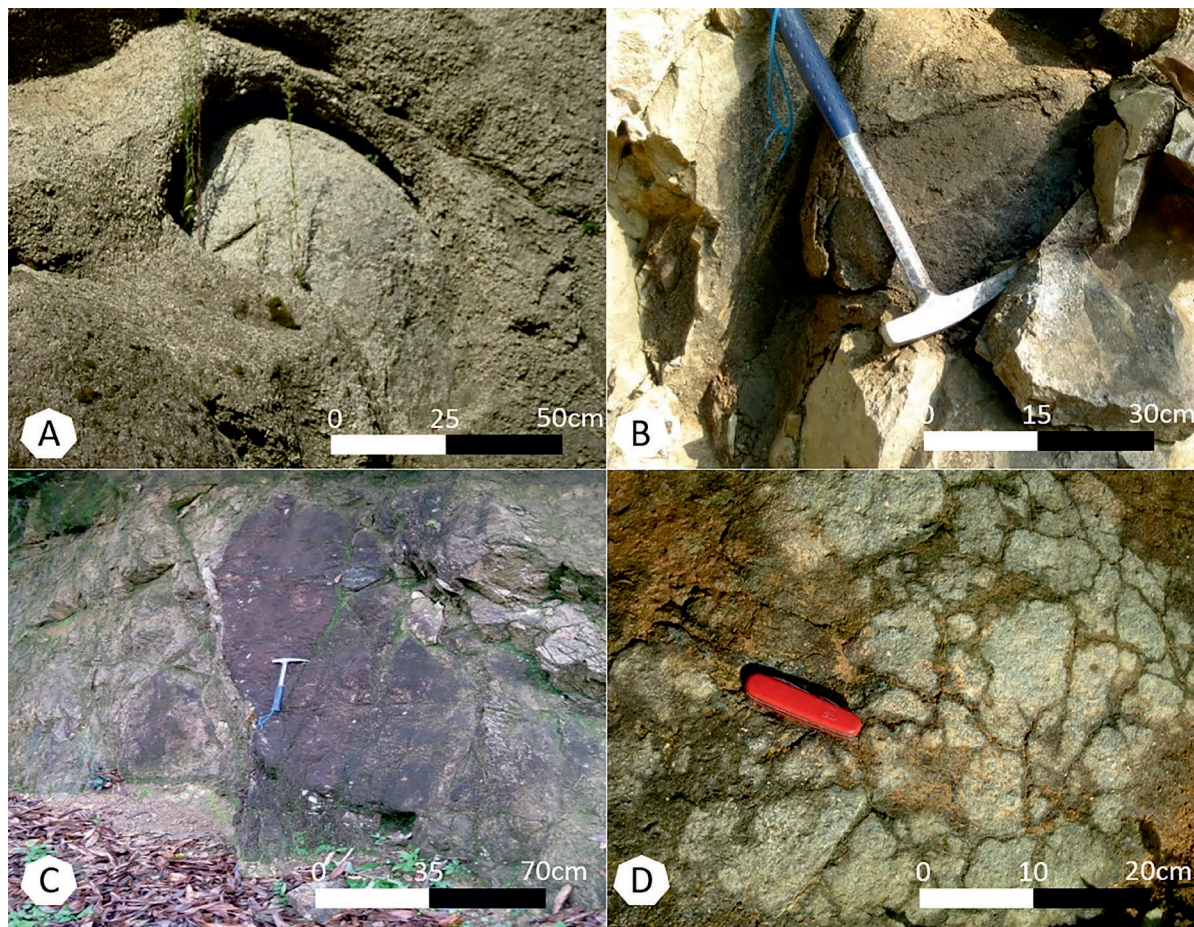


Fig. 4. Field photographs: **A** — Upper Paleozoic xenolith of biotite-bearing granite (312 ± 6.6 Ma) in the Namonastrevi syenite pluton (42.42 ± 0.52 Ma); **B** — Undated mafic microgranular enclave in the Merisi syenite pluton; **C** — Gabbroic restite (46.77 ± 0.81 Ma) in the Zoti syenite pluton (43.86 ± 0.43 Ma); **D** — Mg-rich tholeiitic basaltic xenolith with inherited zircon grains (515 ± 9 Ma; 632 ± 29 Ma; 747 ± 33 Ma) in the Vakijvari syenite pluton (43.26 ± 0.74 Ma).

Mafic microgranular enclaves are found in almost all plutons of the Adjara–Trialeti belt. They range in shape from spheroidal to ellipsoidal, from fine-grained to micro-granular, and from a centimetre- to decimetre-scale in size (Fig. 4). The contact between mafic microgranular enclaves and surrounding plutonic rocks is sharp and sometimes is surrounded by light coloured alteration rim. The mafic microgranular enclaves mainly consist of plagioclase (>50 %), biotite (10–20 %), K-feldspar (10–15 %) and quartz (5–10 %), as well as accessory apatite, magnetite and allanite. However, the southern periphery of the Zoti pluton contains dark-coloured, hornblende-pyroxene restite (~2 m×1 m; Fig. 4), from which we were able to separate and date zircon grains.

Zircons U–Pb geochronology

Methodology

A suite of 20 igneous rock samples (~5 kg each) were collected along the Adjara–Trialeti belt for zircon separation and

U–Pb geochronology. Enough zircon grains were separated from only 15 samples and a total of 342 separated zircons were dated. Unfortunately, we could not separate zircons from the mafic microgranular enclaves. The U–Pb zircon geochronology was conducted at the Department of Geosciences, National Taiwan University, Taipei, Taiwan, equipped with an Agilent 7500s quadrupole ICP–MS and a New Wave UP213 laser ablation system. Calibrations were performed using the GJ-1 zircon standard (Jackson et al. 2004) and Plešovice zircon (Sláma et al. 2008) to assess data quality. All the U–Th–Pb isotope ratios were calculated using GLITTER 4.4.2 (GEMOC) software, and the isotope ratio of common lead corrected using the approach proposed by Andersen (2002). Isoplot v. 3.0 (Ludwig 2003) was used to calculate weighted mean U–Pb ages and probability density curves. The detailed analytical procedure has been described by Chiu et al. (2009).

Crystallization ages of Eocene plutons

A total of 204 analysed zircons from the Adjara–Trialeti plutons have zoned textures, prismatic shapes, and lengths

which range from 80 and 140 μm . Their Th/U ratios exceed 0.4, which is typical for zircons of magmatic origin (Wu et al. 2004).

Two samples have been dated from the Merisi pluton. The first – 12GE03 – is taken from the western periphery of the pluton and represents a fine-grained, equigranular, hypidiomorphic, hornblende-bearing monzonite. Twenty zircon grains that were dated from this sample yield a weighted mean $^{206}\text{Pb}/^{238}\text{U}$ age of 43.42 ± 0.61 Ma, MSWD=1.6. The second one – 12GE04 – is taken in 150 m east of the first one and represents a fresh, fine-grained, hypidiomorphic, hornblende-biotite syenite. Twenty-two zircon grains were dated from this sample, yield a weighted mean $^{206}\text{Pb}/^{238}\text{U}$ age of 42.78 ± 0.65 Ma, MSWD=1.6.

Two samples have also been dated from the Namonastrevi pluton. Sample 12GE05 is a fine-grained, hypidiomorphic, pyroxene-biotite syenite. From this sample 22 dated zircon grains yielded a weighted mean $^{206}\text{Pb}/^{238}\text{U}$ age of 42.42 ± 0.52 Ma, MSWD=1.6 (Table 1; Fig. 5).

Another sample (12GE06) is a fine-grained, hypidiomorphic, hornblende quartz-monzonite, which outcrops ~200 m east of sample 12GE05. A total of 11 dated zircon grains yielded a weighted mean $^{206}\text{Pb}/^{238}\text{U}$ age of $42.03\text{--}0.83$ Ma (MSWD=1.3). Both ages are interpreted as the magma crystallization ages.

One sample (12GE13) was taken from the Vakijvari pluton, in the Bjuja gorge, along the Shemokmedi–Gomi motorway. It is a fine-grained, hypidiomorphic, fresh, massive, hornblende-biotite syenite. 22 zircon separated from this sample were dated to yield a weighted mean $^{206}\text{Pb}/^{238}\text{U}$ age to 43.26 ± 0.74 Ma, MSWD=1.9 (Fig. 5).

One sample (12GE14) was dated from the Zoti pluton from the river Tetri-Gele River valley. It is fine-grained, hypidiomorphic, massive, crushed, pyroxene-biotite syenite. 24 zircon grains from the syenite sample were dated to yield a weighted mean $^{206}\text{Pb}/^{238}\text{U}$ age of 43.86 ± 0.43 Ma, MSWD=1.01 (Fig. 5).

One sample (12GE19) was dated from the Okros Gele pluton. It is a medium-grained, hypidiomorphic, fresh, massive hornblende-biotite syenite. Twenty-two zircon grains were dated from this sample and yield a weighted mean $^{206}\text{Pb}/^{238}\text{U}$ age of 44.34 ± 0.55 Ma, MSWD=2.1.

A pyroclastic sample of trachyte (12GE10), and a basalt overflow sample (12GE11) from the Acharistskali river valley were dated. A weighted mean $^{206}\text{Pb}/^{238}\text{U}$ age of the trachytic pyroclastic sample is 50.0 ± 4.8 Ma based on the analysis of 26 zircons grains (MSWD=1.6), whereas the basaltic flow sample crystallized at 42.81 ± 1.52 Ma (9 zircon grains; MSWD=0.0086).

Ages of xenoliths and restites

Two restites and three xenolith samples were dated using the LA-ICP-MS U–Pb zircon technique. No zircons were found in the mafic microgranular enclaves. A total of 120 zircon grains were dated from restites and xenoliths. These grains have similar zonal textures, prismatic shapes and lengths ranging from 50 to 120 μm . The zircon grains from restite samples have Th/U ratio greater than 0.4 as opposed to those from granite xenoliths (Th/U ratio <0.4).

A weighted mean $^{206}\text{Pb}/^{238}\text{U}$ age of 312.1 ± 6.6 Ma, MSWD=3.0 was obtained from 24 concordant zircon grains

Table 1: Zircons U–Th chemical analyses, U–Pb ratios and ages of the Namonastrevi pluton (12Ge-05 sample) (weighted mean $^{206}\text{Pb}/^{238}\text{U}$ age 42.42 ± 0.52 Ma).

Spot	U (ppm)	Th/U	U–Pb ratios			Ages (Ma)			Inferred age (Ma)
			$^{206}\text{Pb}/^{238}\text{U}$	$^{207}\text{Pb}/^{206}\text{Pb}$	$^{207}\text{Pb}/^{235}\text{U}$	$^{206}\text{Pb}/^{238}\text{U}$	$^{207}\text{Pb}/^{206}\text{Pb}$	$^{207}\text{Pb}/^{235}\text{U}$	
1	841.0	1.1410	0.00649	0.04805	0.04299	41.7	102	43	41.7
2	198.8	0.7636	0.00704	0.04531	0.04397	45	-4	44	45
3	2149.9	2.3636	0.00648	0.04849	0.0433	41.6	123	43	41.6
4	360.7	0.8632	0.00629	0.04585	0.03978	40.4	-10	40	40.4
5	780.6	1.1410	0.00666	0.04864	0.04429	42.4	131	44	42.4
6	359.4	0.6090	0.00671	0.04789	0.04429	43.1	94	44	43.1
7	366.8	0.6707	0.00642	0.04799	0.04248	41.3	99	42	41.3
8	366.1	0.7142	0.00669	0.04841	0.04466	43	119	44	43
9	1377.7	1.6825	0.00643	0.05005	0.04435	41.3	197	44	41.3
10	563.8	0.9107	0.00635	0.04609	0.04033	40.8	2	40	40.8
11	360.0	0.7464	0.00655	0.04708	0.0425	42.1	53	42	42.1
12	344.0	0.8632	0.00666	0.04819	0.04424	42.8	109	44	42.8
13	259.2	1.0561	0.00649	0.05227	0.04674	41.7	297	46	41.7
14	272.1	1.2256	0.00656	0.04845	0.04385	42.2	121	44	42.2
15	328.2	0.8558	0.00657	0.04718	0.04275	42.2	58	43	42.2
16	365.4	0.7520	0.00661	0.04803	0.04376	42.5	101	43	42.5
17	166.2	0.5366	0.00666	0.04944	0.0454	42.8	169	45	42.8
18	333.3	0.9638	0.00664	0.04608	0.04216	42.6	2	42	42.6
19	291.8	0.6531	0.00687	0.04629	0.04387	44.2	13	44	44.2
20	478.5	1.0341	0.00671	0.05543	0.05126	43.1	430	51	43.1
21	329.7	0.7636	0.00686	0.04762	0.04503	44.1	80	45	44.1
22	407.9	0.7353	0.0067	0.04566	0.04221	43	-20	42	43

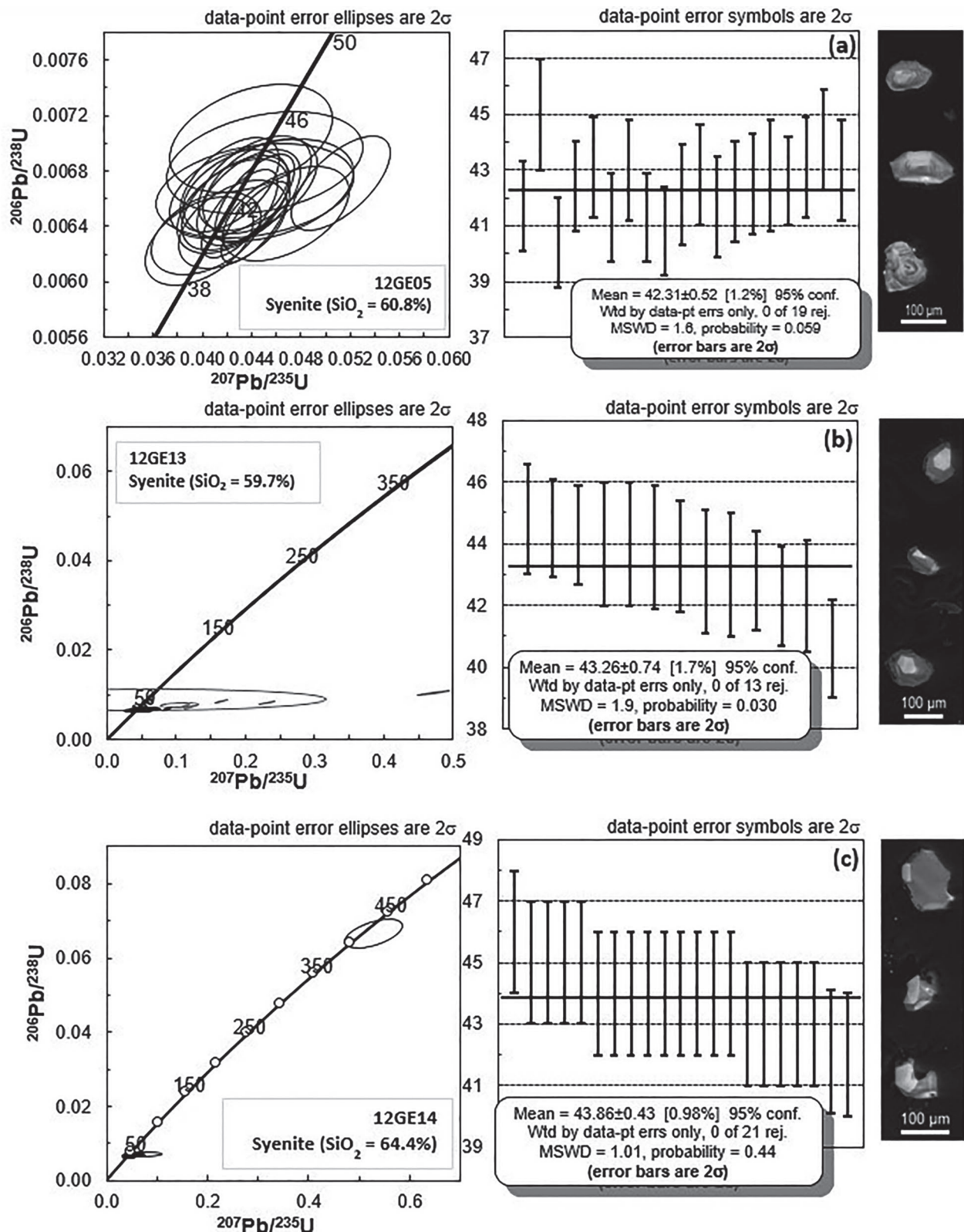


Fig. 5. Concordia plots (left panels), weighted mean $^{206}\text{Pb}/^{238}\text{U}$ ages (central panels), and LA-ICP-MS cathodoluminescence images (right panels) of syenites of the Namonastrevi (a), Vakijvari (b), and Zoti (c) plutons.

Table 2: Zircons U–Th chemical analyses, U–Pb ratios and ages of two-mica granite xenolith (12Ge-09 sample) of the Namonastrevi syenite pluton (weighted mean $^{206}\text{Pb}/^{238}\text{U}$ age of 312.1 ± 6.6 Ma).

Spot	U (ppm)	Th/U	U–Pb ratios			Ages (Ma)			Inferred age (Ma)
			$^{206}\text{Pb}/^{238}\text{U}$	$^{207}\text{Pb}/^{206}\text{Pb}$	$^{207}\text{Pb}/^{235}\text{U}$	$^{206}\text{Pb}/^{238}\text{U}$	$^{207}\text{Pb}/^{206}\text{Pb}$	$^{207}\text{Pb}/^{235}\text{U}$	
1	920.7	0.1558	0.05132	0.05713	0.40426	323	497	345	323
2	861.8	0.1310	0.05488	0.05327	0.40312	344	340	344	344
3	1761.8	0.0950	0.04956	0.05262	0.35953	312	312	312	312
4	260.5	1.0909	0.07863	0.05923	0.64207	488	576	504	488
5	143.1	0.7142	0.079	0.06122	0.66681	490	647	519	490
6	677.1	0.0828	0.04979	0.05326	0.3656	313	340	316	313
7	3314.8	0.0825	0.05092	0.05627	0.395	320	463	338	320
8	2646.5	0.0847	0.05047	0.05216	0.36301	317	292	314	317
9	3661.9	0.1367	0.04938	0.0529	0.36021	311	325	312	311
10	1070.0	0.1811	0.05275	0.05696	0.41421	331	490	352	331
11	712.7	0.0463	0.05628	0.05345	0.41474	353	348	352	353
12	447.6	0.1274	0.09579	0.05968	0.78816	590	592	590	590
13	2323.4	0.0033	0.04753	0.05291	0.3467	299	325	302	299
14	964.0	0.2735	0.05088	0.05678	0.39827	320	483	340	320
15	447.7	0.3732	0.07956	0.0573	0.62847	493	503	495	493
16	1105.9	0.1119	0.04829	0.05525	0.36782	304	422	318	304
17	3704.1	0.2981	0.0468	0.05315	0.34292	295	335	299	295
18	711.0	0.1332	0.05198	0.05494	0.39366	327	410	337	327
19	596.3	0.2014	0.05108	0.05317	0.37442	321	336	323	321
20	1167.0	0.2812	0.0577	0.05925	0.47135	362	576	392	362
21	5573.3	0.1257	0.04656	0.05323	0.34174	293	338	298	293
22	3106.7	0.1677	0.05063	0.0528	0.36853	318	320	319	318

of a two-mica granite xenolith (12GE09) from the Namonastrevi pluton (Table 2; Fig. 6). It should be noted that granites of the same genetic type (two-mica anatectic) and age (Late Variscan) comprise the significant part of the Dzirula and Khrami massifs of the Transcaucasus microplate (Okrostsvardize & Clarke 2004; Gamkrelidze & Shengelia 2005; Chiu et al. 2015).

The weighted mean $^{206}\text{Pb}/^{238}\text{U}$ age at 473.8 ± 4.5 Ma, MSWD=3.6 was obtained from 24 zircon grains from a hornblende-biotite granodiorite xenolith of the Namonastrevi pluton (12GE08) (Table 1; Fig. 6). It should be noted that these data are similar to those for the ages and petrography of granodiorite that have been reported from the Dzirula and Khrami massifs of the Transcaucasus microplate (Okrostsvardize & Clarke 2004; Gamkrelidze & Shengelia 2005; Chiu et al. 2015).

One sample of gabbroic restite (12GE16) was dated from the Zoti pluton (Table 3; Fig. 6). The sample is a piece of dark-coloured, massive, fresh, olivine containing pyroxene-hornblende gabbro. From this sample twenty-four dated zircon grains give a weighted mean $^{206}\text{Pb}/^{238}\text{U}$ age of 46.77 ± 0.81 Ma, MSWD=2.9.

One sample of gabbroic restite (12GE21) was dated from the Okros Gele pluton. It is a piece of dark-coloured, fresh, massive, hornblende-clinopyroxene gabbro. From this sample twenty-four dated zircon grains give a weighted mean $^{206}\text{Pb}/^{238}\text{U}$ age of 44.85 ± 0.59 Ma, MSWD=1.65.

One sample (19GE19) was dated from the Rkviana gabbroic restite which comprises hornblende-pyroxene porphyritic rock. From this sample twenty-four dated zircon grains

give a weighted mean $^{206}\text{Pb}/^{238}\text{U}$ age of 44.85 ± 0.59 Ma, MSWD=1.65.

One sample from an oval-shaped basalt xenolith (12GE12), has been dated from the Vakijvari pluton. The sample was taken along the Shemokmedi–Gomi motorway and is a piece of dark-coloured, massive, crushed olivine-augite rock. Twenty-six zircon grains were separated and dated from this sample. The weighted mean $^{206}\text{Pb}/^{238}\text{U}$ ages were as follows: (1) 515.4 ± 9.5 Ma, MSWD=0.76 (4 grains); (2) 632 ± 29 Ma, MSWD=3.7 (5 grains); and (3) 747 ± 33 Ma, MSWD=5.1 (6 grains) (Table 4; Fig. 6).

Petrochemistry of the plutons and their enclaves

Among the collected rock samples, 12 fresh ones of the Adjara–Trialeti plutons and their xenoliths and restites were selected for the chemical analysis of the whole-rock compositions, using an X-ray fluorescence spectrometer (XRF 2000) at the Geological Institute of the Tbilisi State University, Georgia (Table 5). These results allowed us to investigate some petrochemical features of dated samples (Fig. 7).

On the TAS discrimination diagram the main magmatic phases of all the plutons is predominantly represented by monzonites and syenites. In these rocks the silica (SiO_2) content varies between 55 and 70 wt. %, whereas the alkali content ($\text{Na}_2\text{O}+\text{K}_2\text{O}$) is commonly more than 8 wt. %. In the plutons the rocks of mafic composition are represented by minor gabbroic, gabbro-dioritic and monzo-dioritic phases (Fig. 7a).

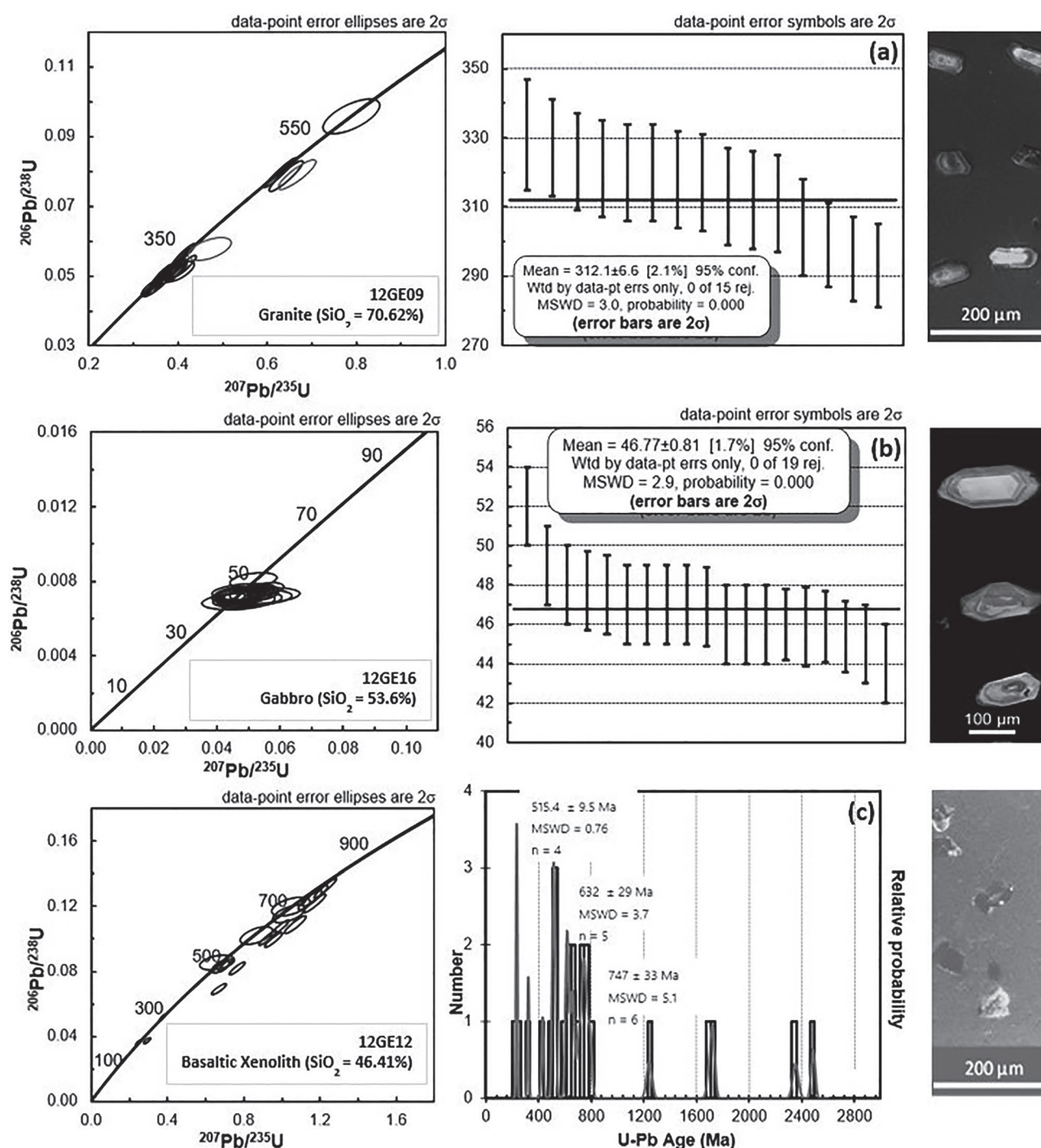


Fig. 6. Concordia plots (left panel), weighted mean $^{206}\text{Pb}/^{238}\text{U}$ ages (central panel), and cathodoluminescence images (right panel) of the Namonastrevi pluton granite xenolith (a), Zoti pluton gabbroic restite (b), and inherited zircons of basaltic xenolith of the Vakijvari pluton (c).

In these rocks the silica content (SiO_2) varies from 46 to 54 wt. %, whereas the alkali content ($\text{Na}_2\text{O} + \text{K}_2\text{O}$) is less than 5 wt. % (Table 5).

The Adjara–Trialeti plutons and their enclaves are placed in different fields of AFM discrimination diagrams. The samples of the main felsic magmatic phase of these plutons are

placed in the field of dacite of calc-alkaline series, whereas the samples of mafic enclaves are placed in the field of basalt of tholeiitic series (Fig. 7b).

The main felsic magmatic phase of the plutons fall in the field of post-collision granites, whereas the granitic xenoliths are in the field of syn-collision granites. The mafic

enclaves are placed in the field of volcanic arc granites, and the basaltic xenolith is placed in the field of within plate granites (Fig. 7c).

These rocks are also placed in different fields on the Hf–Rb/30-Ta*3 discrimination diagram and show the similar pattern as on the previous diagram (Fig. 7d). Data representing

the felsic magmatic phase of plutons are mainly placed in the field of post-collision granite, the granitic xenoliths – in the field of syn-collision granites, the mafic enclaves are placed in the fields of volcanic arc and post-collision granites, whereas basaltic xenolith falls in the field of within plate granites (Fig. 7).

Table 3: Zircons U–Th chemical analyses, U–Pb ratios and ages of the diorite restite (12Ge-16 sample) of the Zoti pluton (weighted mean $^{206}\text{Pb}/^{238}\text{U}$ age 46.77 ± 0.81 Ma).

Spot	U (ppm)	Th/U	U–Pb ratios			Ages (Ma)			Inferred age (Ma)
			$^{206}\text{Pb}/^{238}\text{U}$	$^{207}\text{Pb}/^{206}\text{Pb}$	$^{207}\text{Pb}/^{235}\text{U}$	$^{206}\text{Pb}/^{238}\text{U}$	$^{207}\text{Pb}/^{206}\text{Pb}$	$^{207}\text{Pb}/^{235}\text{U}$	
1	1087.0	0.6488	0.00714	0.04818	0.04746	45.9	108	47	45.9
2	199.2	0.6531	0.00729	0.04608	0.04633	47	2	46	47
3	110.0	0.3677	0.00701	0.0512	0.04951	45	250	49	45
4	459.5	0.8708	0.0073	0.0464	0.0467	47	18	46	47
5	156.9	0.4890	0.00723	0.0544	0.0542	46	388	54	46
6	548.1	0.9365	0.0073	0.0494	0.04969	46.9	167	49	46.9
7	666.6	0.4842	0.00707	0.04651	0.04536	45.4	24	45	45.4
8	427.9	0.6846	0.00733	0.04642	0.04693	47	19	47	47
9	373.7	0.6446	0.00731	0.05031	0.05068	47	209	50	47
10	350.7	0.8413	0.00711	0.05281	0.05174	46	321	51	46
11	188.9	0.4472	0.00693	0.04891	0.04671	44	144	46	44
12	296.8	0.8632	0.0072	0.04831	0.04796	46	115	48	46
13	281.2	0.7879	0.0074	0.04812	0.04909	47.5	105	49	47.5
14	126.5	0.5366	0.00743	0.04779	0.04895	48	89	49	48
15	775.7	1.0027	0.00716	0.05281	0.0521	46	321	52	46
16	194.7	0.5425	0.00756	0.05235	0.05459	49	301	54	49
17	1328.7	0.8485	0.00807	0.04617	0.05137	52	7	51	52
18	360.2	0.4452	0.0864	0.05931	0.70647	534	579	543	534
19	787.9	0.4964	0.00714	0.05172	0.05093	45.9	273	50	45.9
20	445.2	0.7879	0.00742	0.05292	0.05412	47.7	325	54	47.7

Table 4: Zircons U–Th chemical analyses, U–Pb ratios and ages of the Mg-rich basaltic xenolith of the Vakijvari pluton (12Ge-12 sample) (weighted mean $^{206}\text{Pb}/^{238}\text{U}$ ages: (1) 515.4 ± 9.5 Ma; (2) 632 ± 29 Ma; (3) 747 ± 33 Ma).

Spot	U (ppm)	Th/U	U–Pb ratios			Ages (Ma)			Inferred age (Ma)
			$^{206}\text{Pb}/^{238}\text{U}$	$^{207}\text{Pb}/^{206}\text{Pb}$	$^{207}\text{Pb}/^{235}\text{U}$	$^{206}\text{Pb}/^{238}\text{U}$	$^{207}\text{Pb}/^{206}\text{Pb}$	$^{207}\text{Pb}/^{235}\text{U}$	
1	183.8	0.6128	0.18771	0.08182	2.11695	1109	1241	1154	1241
2	793.1	0.1818	0.08317	0.05911	0.67782	515	571	525	515
3	1248.3	0.2920	0.40459	0.16278	9.07967	2190	2485	2346	2485
4	262.7	0.3365	0.1154	0.06511	1.03595	704	778	722	704
5	607.0	0.7817	0.28612	0.10555	4.16366	1622	1724	1667	1724
6	1259.9	0.3365	0.1309	0.06797	1.22664	793	868	813	793
7	757.7	0.2954	0.1019	0.06164	0.86602	626	662	633	626
8	608.5	0.1612	0.06913	0.0703	0.67002	431	937	521	431
9	638.5	0.1970	0.08518	0.05619	0.65994	527	460	515	527
10	345.2	0.2626	0.09942	0.06977	0.95637	611	922	681	611
11	552.4	0.4224	0.11989	0.06328	1.04599	730	718	727	730
12	422.8	0.2928	0.08167	0.06793	0.76483	506	866	577	506
13	360.1	0.3690	0.27771	0.15046	5.76111	1580	2351	1941	2351
14	1869.6	0.0697	0.10061	0.06657	0.92357	618	824	664	618
15	460.9	0.5608	0.10665	0.06715	0.98742	653	842	697	653
16	255.4	0.6846	0.03645	0.04962	0.24936	231	177	226	231
17	277.5	0.5515	0.12192	0.0697	1.17171	742	920	787	742
18	257.8	0.3093	0.10874	0.07121	1.06778	665	963	738	665
19	881.1	0.0949	0.12665	0.06721	1.17357	769	844	788	769
20	237.9	2.0681	0.08369	0.06103	0.70418	518	640	541	518
21	141.8	0.7636	0.28418	0.10461	4.09855	1612	1707	1654	1707
22	2311.2	0.0482	0.03749	0.05706	0.29491	237	494	262	237
23	1149.5	0.0967	0.12367	0.06735	1.14833	752	849	776	752
24	1683.6	0.3182	0.05115	0.05274	0.3719	322	318	321	322

Table 5: The X-ray fluorescence chemical analyses of some major, trace and rare earth elements of the plutonic rocks and their enclaves of the Adjara–Trialeti belt.

Sample	12GE01	12GE03	12GE04	12GE05	12GE08	12GE09	12GE12	12GE13	12GE14	12GE16	12GE19	12GE21
Major elements (wt. %)												
SiO ₂	53.8	60.0	58.9	60.8	64.4	70.6	46.4	61.	64.4	53.6	60.6	48.6
Al ₂ O ₃	18.5	17.3	18.5	17.5	14.2	13.5	12.5	19.54	18.1	18.9	17.3	17.2
Fe ₂ O ₃	8.5	5.7	5.1	5.7	6.7	2.8	10.1	5.1	3.6	8.2	2.1	8.5
CaO	6.1	2.4	3.3	2.5	1.9	1.9	11.6	0.2	0.4	7.7	5.8	10.8
MgO	3.4	1.7	2.1	1.7	3.1	0.8	13.4	0.8	0.4	3.2	2.5	7.9
Na ₂ O	4.1	4.2	5.8	4.8	3.3	3.6	0.3	7.8	5.9	4.2	7.5	2.7
K ₂ O	2.3	4.8	6.5	5.4	3.8	4.3	1.5	5.5	7.4	0.6	1.6	0.6
MnO	0.4	0.3	0.1	0.2	0.1	0.1	1.2	0.1	0.1	0.3	0.1	0.2
TiO ₂	0.9	0.6	0.8	0.7	0.9	0.1	0.7	0.4	0.3	0.7	0.6	0.8
P ₂ O ₅	0.5	0.3	0.4	0.3	0.4	0.4	0.4	0.1	0.1	0.3	0.3	0.1
Trace elements (ppm)												
Co	18.1	11	6.4	6.1	27	42	38.35	3.5	4.2	21	14	27
Hf	4.5	3.7	2.9	1.1	4.2	2.7	1.465	4.3	6.7	3.2	4.3	2.5
Nb	22.6	12.5	30.9	5.9	3.2	5.2	9.68	8.1	9.1	24	11.7	1.5
Rb	125.5	152	175.5	210.4	325	408	25.3	143.5	82	122	147	27
Sr	393.2	497	487.2	249.7	501	609	505.8	157.3	272	336	462	360
Ta	2.	1.2	2.4	3.8	2.3	3.2	3.099	1.5	0.7	2.5	1.4	0.2
Th	12.9	10.7	34.1	12.2	8.7	6.2	4.21	10.5	22.3	14.2	15.7	2.3
U	4.1	3.2	9.6	3.7	4.5	3.0	2.001	4.1	6.7	5.3	3.7	0.6
V	114.0	115	107.9	25.9	70	42	200.9	72	73	112	118	362
W	3.6	2	1.4	1.3	<1	<1	1.773	6.3	1.2	2.7	1.5	0.5

Outcrops and rock types: 12GE01 – Namonastevi pluton, gabbro-diorite; 12GE03 – Merisi pluton, Monzonite; 12GE04 – Merisi pluton, syenite; 12GE05 – Namonastevi pluton, syenite; 12GE08 – Namonastevi pluton, granodioritic xenolith; 12GE09 – Namonastevi pluton, granitic xenolith; 12GE12 – Vakijvari pluton, basaltic xenolith; 12GE13 – Vakijvari pluton, syenite; 12GE14 – Zoti pluton, syenite; 12GE16 – Zoti pluton, monzo-dioritic restite; 12GE19 – Okros Gele pluton, monzonite; 12GE21 – Okros Gele pluton, gabbroic restite.

Results and discussion

The results of the new zircon LA-ICP-MS U–Pb geochronological data of plutonic rocks and their xenoliths and restite from the Adjara–Trialeti belt have been summed up on one chart (Table 6).

Our investigation shows that the deposition of pyroclastic material in the Adjara–Trialeti basin began in the early Eocene (~50 Ma). Gabbroic intrusions were emplaced between ~46 and ~44 Ma, which led to assimilation and contamination of continental type crust and formation of the intermediate melts. About ~43 to ~42 Ma ago, these melts intruded into the volcano-sedimentary cover in some areas and crystallized as plutons of monzo-syenitic composition. Magmatic activity ended with the formation of basaltic lava flows at ~42 Ma. From the beginning to the end, this magmatic activity continued about eight million years, between ~50 and ~42 Ma.

The Eocene monzo-syenite plutons of the Adjara–Trialeti belt contain xenoliths of Paleozoic granites (312±7 to 474±5 Ma), basalts xenoliths that contain inherited zircon grains of the Neo-Proterozoic (747±33 Ma, 632±29 Ma) to Cambrian (515±9 Ma) ages and mafic enclaves (~46–44 Ma).

Our new data show that the microcline granitic xenoliths (312±7 to 474±5 Ma) found in the Eocene plutons along the Adjara–Trialeti belt are coeval and have the same mineralogy and age as the Dzirula massif granites. The massif crops out to the north of this belt and contains Upper Paleozoic

microcline granites (331±21 Ma) (Rb–Sr geochronology; Okrostsvardize & Clarke 2004), 322±13 Ma (Lu–Hf geochronology; Chiu et al. 2015).

As mentioned above, the Adjara–Trialeti belt is bordered to the south by the pre-Jurassic massifs, with granites similar in petrology and age to the granitic xenoliths of the Adjara–Trialeti Eocene plutons. For example, the LA-ICP-MS U–Pb zircon ages of the Paleozoic microcline granites of Natric massif vary between 330 and 294 Ma (Topuz et al. 2010).

As for the Neo-Proterozoic and Cambrian zircon crystals there is a high probability that they represent inherited grains captured by magmas during ascent that cut through the Gondwana-derived old continental crust. A large number of relict inherited zircons of this age were also identified from the Paleozoic Dzirula granitoids and their Hf-isotope model age corresponds to a time span between 700 and 500 Ma (Chiu et al. 2015). These inherited zircons have U–Pb ages and Hf isotopic compositions analogous to those from the Eastern Pontides and NW Iran (Chiu et al. 2016).

At the end of this discussion, we would like to point out that the plutons considered above do not reveal any signs of crystal fractionation; therefore, it should be assumed that the mafic enclaves are most likely the restites of the basic injections. This view is supported by the fact that the LA-ICP-MS U–Pb ages of zircons are actually similar in both and are ~46 to ~44 Ma.

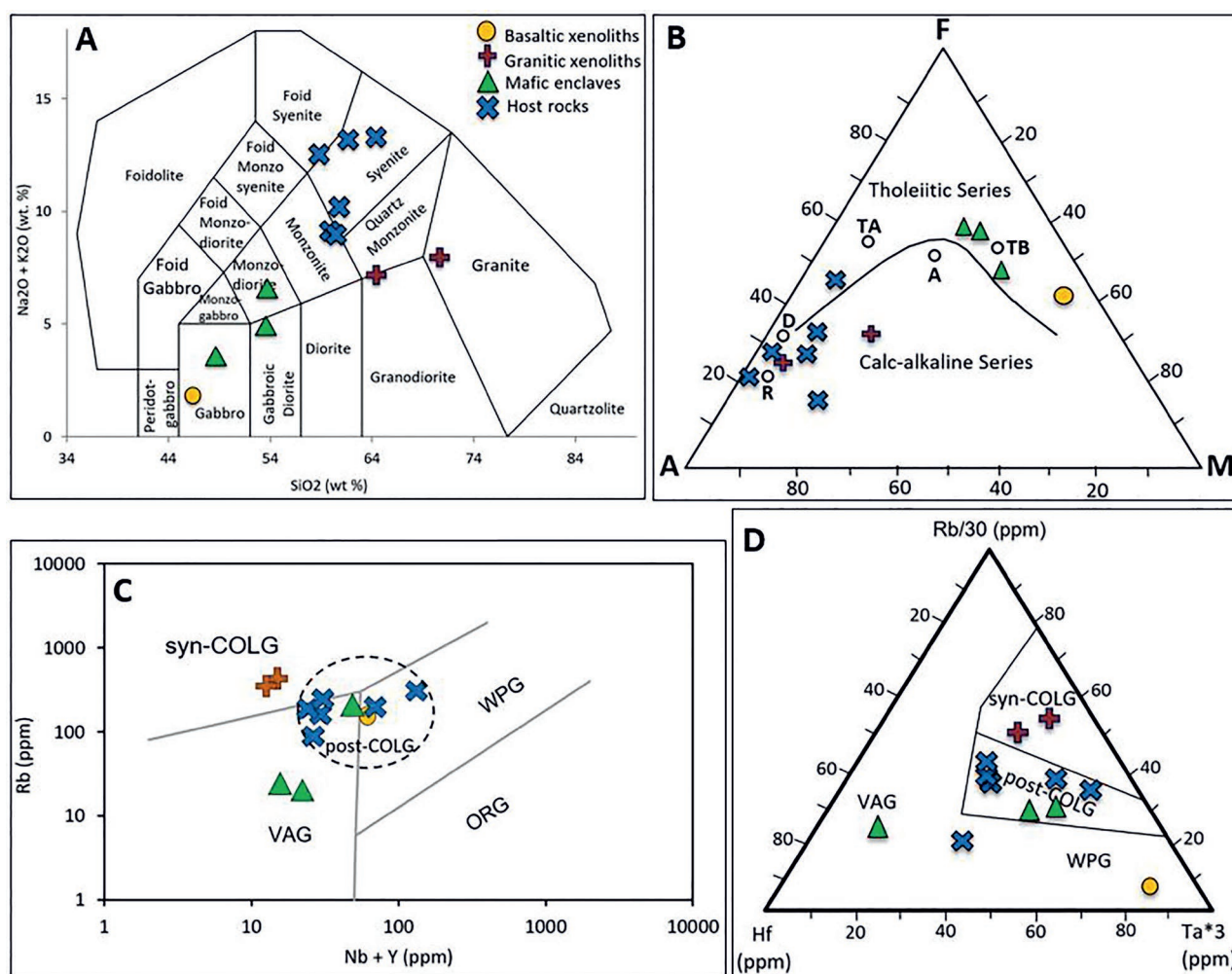


Fig. 7. Petrochemical diagrams for the plutonic rocks and their enclaves of the Adjara–Trialeti belt. **a** — TAS discrimination diagram (Middlemost 1994); **b** — AFM discrimination diagram (Irvine & Baragar 1971) (A=Na₂O+K₂O wt. %; F=FeO total wt. %; M=MgO wt. %). Abbreviations for average compositions: TA — tholeiitic andesites, TB — tholeiitic basalts, A — andesites, D — dacites and R — rhyolites; **c** — Rb–(Nb+Y) geodynamic discrimination diagram (Pearce 1996); **d** — Hf–Rb/30–Ta*30 geodynamic discrimination diagram (Harris et al. 1986). Abbreviations: syn-COLG=syn-collision granite; post-COLG=post-collision granite; VAG=volcanic arc granite; WPG=within-plate granite; ORG=ocean ridge granite.

Conclusions

Based on the results of LA-ICP-MS U–Pb zircon geochronology of the Adjara–Trialeti belt, we can conclude that volcanic activity in the basin began in the Early Eocene, ~50 Ma ago. About ~46 to ~44 Ma ago, the gabbroic magmas were intruded into continental type crust and led to interaction between mantle-derived injections and crust. This process caused the formation of melts of monzonitic to syenitic composition. At ~43 to ~42 Ma ago, these magmas were embedded into the volcano-sedimentary sequence and crystallized in the upper crust. The magmatic activity ended ~42 Ma with the formation of basaltic overflows. In total, the magmatic activity lasted for about eight million years.

Xenoliths occur in the Eocene plutons as the Lower Palaeozoic (312.1±6.6 Ma) and Upper Palaeozoic (473.8±4.5 Ma) granites as well as magnesium-rich basalts with the inherited

zircon grains from the Neoproterozoic to the Cambrian (747±33 Ma, 632±29 Ma, 473.8±4.5 Ma).

The zircon geochronology of the Eocene plutonic xenoliths and regional geological analysis demonstrate that the rift basin of the Adjara–Trialeti belt developed on the pre-Jurassic crystalline basement at the south-western edge of the Transcaucasus microplate, which is consistent with the previously expressed opinion (Gamkrelidze 1986).

Our petrochemical studies suggest, that Eocene monzo-syenite plutons of the Adjara–Trialeti belt and xenoliths of Paleozoic granites belong to the calc-alkaline series, whereas the restites and basalt xenoliths belong to the tholeiitic series. The Paleozoic granite xenoliths belong to the syn-collisional geodynamic settings, similar to the adjacent Dzirula, Khrami and Nartc massifs granites. However, the Eocene monzo-syenite plutons belong to the post-collisional geodynamic settings.

Table 6: Summary of LA-ICP-MS U–Pb zircon dating results of plutons and their enclaves of the Adjara–Trialeti belt.

Sample	Location	Lat (°N)	Long (°E)	Petrography	Age (Ma) ¹	MSWD ²	n ³	Rocks type
12GE03	Merisi pluton	41.5834	41.9661	Monzonite	43.4±0.6	1.6	20	Main phase
12GE04	Merisi pluton	41.5835	41.9681	Syenite	42.8±0.7	1.6	22	Main phase
12GE05	Namonastrevi pluton	41.5768	42.0193	Quartz-Monzonite	42.4±0.5	1.6	22	Main phase
12GE06	Namonastrevi pluton	41.5753	42.0213	Syenite	42.0±0.8	1.3	13	Main phase
12GE08	Namonastrevi pluton	41.5695	42.0263	Grano-diorite	474±5	3.6	24	Xenolith
12GE09	Namonastrevi pluton	41.5690	42.0263	Granite	312±7	3.0	24	Xenolith
12GE10	Pyroclastic rocks	41.5689	41.6722	Trachyte	50.0±4.8	1.6	26	Main phase
12GE11	Basaltic flow	41.5700	41.8679	Bazalt	42.8±1.5	0.08	9	Main phase
12GE12	Vakijvari pluton	41.8471	42.1252	Basalt	515±10	0.76	6	Xenolith
					632±29	3.7	9	Xenolith
					747±33	5.1	8	Xenolith
12GE13	Vakijvari pluton	41.8533	42.1159	Syenite	43.3±0.7	1.9	22	Main phase
12GE14	Zoti pluton	41.8919	42.4663	Syenite	43.9±0.4	1.01	24	Main phase
12GE16	Zoti pluton	41.8919	42.4663	Gabbro	46.8±0.8	2.9	22	Restite
12GE19	Okros Ghele pluton	41.8813	42.4624	Monzonite	44.3±0.6	2.1	22	Main phase
12GE21	Okros Ghele pluton	41.8834	42.4623	Gabbro	44.8±0.6	1.65	24	Restite
19GE19	Rkviana pluton	41.8515	42.4829	Gabbro	44.5±0.6	1.87	20	Restite

¹ ²⁰⁶Pb/²³⁸U weighted mean ages² Mean square of weighted deviates³ Excluding discordant and outlier spot analyses, and xenocrystic zircons

Considering the fact that the closure of the Northern Neotethyan Ocean occurred either in the Late Cretaceous (Rolland et al. 2012; Meijers et al. 2015) or the Paleocene (Yilmaz et al. 1997; Topuz et al. 2011; Robertson et al. 2013; Moritz et al. 2016) and based on our new data, we assume that the Adjara–Trialeti basin evolved from the Late Cretaceous to Eocene from a back-arc extensional regime -to post-collision geodynamic setting.

Acknowledgements: This research was supported by the Shota Rustaveli National Science Foundation of Georgia (SRNSFG) [grant #FR-18-8122] and the Inter-Geological Grant within the scope of the “Silk Road Project (II): Tibet/Himalaya vs. Caucasus/Iran Orogenic Belts”. We are grateful to Dr. Igor Petrik whose thoughtful comments and constructive suggestions helped to improve the earlier version of the manuscript.

References

- Agamalian V. 2004: The Lesser Caucasus earth crust formation and evolution in the collision zone of Palaeo-Tethys. In: Proceedings of the 5th International Symposium on Eastern Mediterranean Geology, 17–20.
- Andersen T. 2002: Correction of common lead in U–Pb analyses that do not report ²⁰⁴Pb. *Chemical Geology* 192, 59–79. [https://doi.org/10.1016/S0009-2541\(02\)00195-X](https://doi.org/10.1016/S0009-2541(02)00195-X)
- Ashwal L., Torsvik T., Horvath P., Harris C., Webb S., Werner S. & Corfu F. 2016: A mantle-derived origin for Mauritian trachytes. *Journal of Petrology* 57, 1645–1676. <https://doi.org/10.1093/ptrology/egw052>
- Asiabanha A. & Foden J. 2012: Post-collisional transition from an extensional volcano-sedimentary basin to a continental arc in the Alborz Ranges, N-Iran. *Lithos* 148, 98–111. <https://doi.org/10.1016/j.lithos.2012.05.014>
- Balavadze B., Tvaltvaladze G., Shengelaia G., Sikharulidze D. & Kartvelishvili M. 1966: Geophysical investigation of the Earth's crust within the Caucasus. *Journal of Geotectonica* 3, 34–43 (in Russian).
- Ballato P., Uba C.E., Landgraf A., Strecker M.R., Sudo M., Stockli D.F., Friedrich A. & Tabatabaei S.H. 2011: Arabia-Eurasia continental collision: Insights from Late Tertiary foreland-basin evolution in the Alborz Mountains, northern Iran. *Geological Society of America Bulletin* 123, 106–131. <https://doi.org/10.1130/B30091.1>
- Barbarin B. 2005: Mafic magmatic enclaves and mafic rocks associated with some granitoids of the central Sierra Nevada batholith, California: nature, origin, and relations with the hosts. *Lithos* 80, 155–177. <https://doi.org/10.1016/j.lithos.2004.05.010>
- Chiu H.Y., Chung S.L., Wu F.Y., Liu D., Liang Y.H., Lin I.J., Iizuka Y., Xie L.W., Wang Y. & Chu M.F. 2009: Zircon U–Pb and Hf isotope constraints from eastern Transhimalayan batholiths on the precollisional magmatic and tectonic evolution in southern Tibet. *Tectonophysics* 477, 3–19. <https://doi.org/10.1016/j.tecto.2009.02.034>
- Chiu H.Y., Chung S.L., Shengelia D., Okrostsvaridze A., Wu F.Y., Lee H.Y. & Iizuka Y. 2015: Zircon Hf isotopic constraints on the petrogenesis of the Dzirula complex in Georgian Caucasus: the existence of Arabian micro-continents. Abstract of Goldschmidt 2015 Conference, Prague, Czech Republic. <https://goldschmidt-abstracts.info/2015/540.pdf>
- Chiu H.Y., Chung S.L., Okrostsvaridze A., Javakhishvili Z., Lee H.Y. & Wang K. L. 2016: Discovery of ANS-derived ribbon continent in Georgian Caucasus: Zircon Hf isotopic constraints and implications for the Cimmerian orogeny. Abstract of Goldschmidt 2016 Conference, Yokohama, Japan. <https://goldschmidtabstracts.info/2016/483.pdf>
- Chung S. L., Chu M. F., Zhang, Y., Xie Y., Lo C.H., Lee T.Y., Lan C.Y., Li X., Zhang Q & Wang Y. 2005: Tibetan tectonic evolution inferred from spatial and temporal variations in post-collisional magmatism. *Earth-Science Reviews* 68, 173–196. <https://doi.org/10.1016/j.earscirev.2004.05.001>

- DePaolo D. & Managa M. 2003: Deep Origin of Hotspots – the Mantle Plume Model. *Science* 300, 920–921. <https://doi.org/10.1126/science.1083623>
- Didier J. 1973: Granites and their enclaves. *Elsevier*, 1–393.
- Didier J. & Barbarin B. (Eds.) 1991: Enclaves and granite petrology (Developments in petrology). *Elsevier Science Publishers*, 1–626.
- Dilek Y., Imamverdiyev N. & Altunkaynak S. 2010: Geochemistry and tectonics of Cenozoic volcanism in the Lesser Caucasus (Azerbaijan) and the peri-Arabian region: Collision-induced mantle dynamics and its magmatic fingerprint. *International Geology Review* 52, 4–6. <https://doi.org/10.1016/j.igg.2018.01.003>
- Dudaori O. & Togonidze M. 2016: Petrology and isotope geochronology of Mesozoic intrusive complexes of Georgia. *Proceedings of Janelidze Institute of Geology* 128, 1–338.
- Duggen S., Hoernle K., Bogaard P. & Garbe-Schonberg D. 2005: Post-collisional transition from subduction-to intraplate-type magmatism in the westernmost Mediterranean: evidence for continental-edge delamination of subcontinental lithosphere. *Journal of Petrology* 46, 1155–1201. <https://doi.org/10.1093/petrology/egi013>
- Gamkrelidze I. 1974: The most important features of tectonic development of the Anatolian-Caucasian-Iranian segment of the Mediterranean belt. *Report of Georgian Academy of Sciences SSR* 74, 117–120.
- Gamkrelidze I. 1976: Mechanism of formation of tectonic structures and some common problems of tectogenesis. *Mecniereba*, 1–219.
- Gamkrelidze I. 1986: Geodynamic evolution of the Caucasus and adjacent areas in Alpine time. *Tectonophysics* 127, 261–277.
- Gamkrelidze I. 2003: Geological Map of Georgia. Scale 1:50,000. *Georgian State Department of Geology*.
- Gamkrelidze I.P. & Shengelia D.M. 2005: The Precambrian-Paleozoic regional metamorphism, magmatism and geodynamics of the Caucasus. *Scientific World*, 1–458.
- Gamkrelidze I.P., Dumbadze G.D. & Kekelia M.A. 1981: Ophiolites of the Dzirula massif and problem of Paleotethyse in Caucasus. *Geotectonic* 5, 23–33.
- Gamkrelidze I., Shengelia D., Lee Y. H., Okrostsvaridze A., Beridze G. & Vardanashvili K. 2020: U–Pb LA–ICP–MS dating of zoned zircons from the Greater Caucasus pre-Alpine crystalline basement: Evidence for Cadomian and Variscan evolution. *Geologica Carpathica* 71, 249–263. <https://doi.org/10.31577/Geol-Carp.71.3.4>
- Griffin W.L., Wang X., Jackson S.E., Pearson N.J., O'Reilly S.Y., Xu X.S. & Zhou X.M. 2002: Zircon chemistry and magma mixing, SE China: in-situ analysis of Hf isotopes, Tonglu and Pingtan igneous complexes. *Lithos* 61, 237–269. [https://doi.org/10.1016/S0024-4937\(02\)00082-8](https://doi.org/10.1016/S0024-4937(02)00082-8)
- Harris N., Pearce J. & Tindle A.G. 1986: Geochemical characteristics of collision-zone magmatism. *Geological Society, Special Publications* 19, 67–81. <https://doi.org/10.1144/GSL.SP.1986.019.01.04>
- Irvine T. N. & Baragar W. R. 1971: A guide to the chemical classification of the common volcanic rocks. *Canadian Journal of Earth Sciences* 8, 523–548. <https://doi.org/10.1139/e71-055>
- Jackson S., Pearson N., Griffin W. & Belousova E. 2004: The application of laser ablation–inductively coupled plasma–mass spectrometry to in situ U–Pb zircon geochronology. *Chemical Geology* 211, 47–69. <https://doi.org/10.1016/j.chemgeo.2004.06.017>
- Keskin M., Pearce J.A., Kempton P.D. & Greenwood P. 2006: Magma-crust interactions and magma plumbing in a post-collision setting: geochemical evidence from the Erzurum-Kars Plateau, Eastern Turkey. *Special Paper of the Geological Society of America* 409, 475–505. [https://doi.org/10.1130/2006.2409\(23\)](https://doi.org/10.1130/2006.2409(23))
- Laliev A.F. & Zirakadze M.U. 1971: New data on the geological structure of the Chikhati anticline. *Bulletin of the Academy of Sciences of Georgia* 61, 52–57 (in Russian with English abstract).
- Liu L., Qiu J.S. & Li Z. 2013: Origin of mafic microgranular enclaves (MMEs) and their host quartz monzonites from the Muchen pluton in Zhejiang Province, Southeast China: implications for magma mixing and crust-mantle interaction. *Lithos* 160, 145–163. <https://doi.org/10.1016/j.lithos.2012.12.005>
- Lordkipanidze M. 1980: Alpine volcanism and geodynamics of the central segment of the Mediterranean belt. *Mecniereba*, 1–162 (in Russian with English abstract).
- Lordkipanidze M., Zakariadze G. & Popolitov E. 1979: Volcanic evolution of marginal and inter-arc basins. *Tectonophysics* 57, 71–83. [https://doi.org/10.1016/0040-1951\(79\)90102-1](https://doi.org/10.1016/0040-1951(79)90102-1)
- Ludwig K.R. 2003: User's manual for Isoplot 3.00: a geochronological toolkit for Microsoft Excel. *Berkeley Geochronology Center, Special Publication*, 1–4.
- Mederer J., Moritz R., Ulianov A. & Chiaradia M. 2013: Middle Jurassic to Cenozoic evolution of arc magmatism during Neotethys subduction and arc-continent collision in the Kapan zone, southern Armenia. *Lithos* 177, 61–78. <https://doi.org/10.1016/j.lithos.2013.06.005>
- Meijers M.J.M., Smith B., Kirscher U., Mensink M., Sosson M., Rolland Y., Grigoryan, A., Sahakyan L., Avagyan A., Langereis C. & Müller C. 2015: A paleolatitude reconstruction of the south Armenian block (Lesser Caucasus) for the Late Cretaceous: Constraints on the Tethyan realm. *Tectonophysics* 644–645, 197–219. <https://doi.org/10.1016/j.tecto.2015.01.012>
- Middlemost E.A.K. 1994: Naming materials in the magma/igneous rock system. *Earth-Science Reviews* 37, 215–224.
- Moritz R., Melkonyan R., Selby D., Popkhadze N., Gugushvili V., Tayan R. & Ramazanov V. 2016: Metallogeny of the Lesser Caucasus: From Arc Construction to Postcollision Evolution. *Society of Economic Geology, Special Publication* 19, 157–192. <https://doi.org/10.5382/SP.19.06>
- Okay A.I. & Topuz G. 2017: Variscan orogeny of the Black Sea region. *International Journal of Earth Sciences* 106, 569–592. <https://doi.org/10.1007/s00531-016-1395-z>
- Okrostsvaridze A. 2007: Hercynian granitoid magmatism of the Greater Caucasus. *Nekeri*, 1–223 (in Russian with English abstract).
- Okrostsvaridze A. & Clarke D.B. 2004: New Sm–Nd, Rb–Sr and Ar–Ar isotope data of the Dzirul Salient igneous rocks of the Transcaucasus massif. *Report of Academy of Sciences of Russia* 398, 34–40.
- Okrostsvaridze A. & Tormey D. R. 2011: Evolution of the Variscan Orogenic Plutonic Magmatism: The Greater Caucasus. *Journal of Nepal Geological Society, Special Issue* 403, 45–52. <https://doi.org/10.3126/jngs.v43i0.24514>
- Okrostsvaridze A. & Tormey D.R. 2013: Phanerozoic Continental Crust Evolution of the Inner Caucasian Microplate. The Dzirula massif. *Episodes* 36, 31–39. <https://doi.org/10.18814/epiugs/2013/v36i1/005>
- Okrostsvaridze A., Chung S.L., Chang Y.H., Gagnidze N., Boichenko G. & Gogoladze S. 2018: Zircons U–Pb Geochronology of the ore-bearing Plutons of Adjara–Trialeti folded belt, Lesser Caucasus. *Bulletin of the Georgian Academy of Sciences* 12, 90–99.
- Pearce J.A. 1996: Source and setting of granitic rocks. *Episodes* 19, 120–125. <https://doi.org/10.18814/epiugs/1996/v19i4/005>
- Peccerillo A., Barberio M.R., Yirgu G., Ayalew D., Barbieri T. & Wu W. 2003: Relationships between mafic and peralkaline silicic magmatism in continental rift settings: a petrological, geochemical and isotopic study of the Gedemsa volcano, central

- Ethiopian rift. *Journal of Petrology* 44, 2003–2032. <https://doi.org/10.1093/petrology/egg068>
- Philip H., Cisternus A., Gvishiani A. & Gorshkov A. 1989: The Caucasus: An actual example of the initial stages of a continental collision. *Tectonophysics* 161, 1–21. [https://doi.org/10.1016/0040-1951\(89\)90297-7](https://doi.org/10.1016/0040-1951(89)90297-7)
- Rabayrol F., Hart C.J.R. & Thorkelson D.J. 2019: Temporal, spatial and geochemical evolution of late Cenozoic post-subduction magmatism in central and eastern Anatolia, Turkey. *Lithos* 336–337, 67–96. <https://doi.org/10.1016/j.lithos.2019.03.022>
- Richards J.P. 2015: Tectonic, magmatic, and metallogenic evolution of the Tethyan orogeny: from subduction to collision. *Ore Geology reviews* 70, 323–345. <https://doi.org/10.1016/j.oregeorev.2014.11.009>
- Robertson A.H.F., Parlak O. & Ustaömer T. 2013: Late Palaeozoic–early Cenozoic tectonic development of southern Turkey and the easternmost Mediterranean region: Evidence from the inter-relationships of continental and oceanic units. *Geological Society of London Special Publication* 372, 9–48. <https://doi.org/10.1144/SP372.22>
- Rolland Y., Perincek D., Kaymakci N., Sosson M., Barrier E. & Avagyan A. 2012: Evidence for ~80–75 Ma subduction jump during Anatolide-Tauride–Armenian block accretion and ~48 Ma Arabia–Eurasia collision in Lesser Caucasus-east Anatolia. *Journal of Geodynamics* 56–57, 76–85. <https://doi.org/10.1016/j.jog.2011.08.006>
- Sengor A.M.C. & Yilmaz Y. 1981: Tethyan evolution of Turkey: a plate tectonic approach. *Tectonophysics* 75, 181–241. [https://doi.org/10.1016/0040-1951\(81\)90275-4](https://doi.org/10.1016/0040-1951(81)90275-4)
- Shellnutt J.G., Jahn B.M. & Dostal J. 2010: Elemental and Sr–Nd isotope geochemistry of microgranular enclaves from peralkaline A-type granitic plutons of the Emeishan large igneous province, SW China. *Lithos* 119, 34–46. <https://doi.org/10.1016/j.lithos.2010.07.011>
- Sláma J.J., Košler D.J., Condon J.L., Crowley A., Gerdes J.M., Hanchar M.S.A., Horstwood, G.A., Morris L., Nasdala N., Norberg U., Schaltegger B., Schoene M.N. & Whitehouse M.J. 2008: Plešovice zircon – A new natural reference material for U–Pb and Hf isotopic microanalysis. *Chemical Geology* 249, 1–35. <https://doi.org/10.1016/j.chemgeo.2007.11.005>
- Somin M.L. 2011: Pre-Jurassic Basement of the Greater Caucasus. Brief Overview. *Turkish Journal of Earth Sciences* 20, 3–65. <https://journals.tubitak.gov.tr/earth/issues/yer-11-20-5/yer-20-5-2-1008-6.pdf>
- Sosson M., Rolland Y., Müller C., Danelian T., Melkonyan R., Kekelia S., Adamia S., Babzadeh V., Kangarli T., Avagyan A., Galoyan G. & Mosar J. 2010: Subductions, obduction and collision in the Lesser Caucasus (Armenia, Azerbaijan, Georgia), new insights. *Geological Society of London Special Publication* 340, 329–352. <https://doi.org/10.1144/SP340.14>
- Stampfli G.M. & Borel G.D. 2004: A plate tectonic model for the Paleozoic and Mesozoic constrained by dynamic plate boundaries and restored synthetic oceanic isochrones. *Earth and Planetary Science Letters* 196, 17–33. [https://doi.org/10.1016/S0012-821X\(01\)00588-X](https://doi.org/10.1016/S0012-821X(01)00588-X)
- Topuz G., Altherr R., Siebel W., Schwartz W.H., Zack T., Hasözbeke A., Barth B. & Satır M.S. 2010: Carboniferous high-potassium I-type granitoid magmatism in the Eastern Pontides: the Gümüşahane pluton (NE Turkey). *Lithos* 116, 92–110. <https://doi.org/10.1016/j.lithos.2010.01.003>
- Topuz G., Okay A.I., Altherr R., Schwarz W.H., Siebel W., Zack T. & Satır M. 2011: Post-collisional adakite-like magmatism in the Aghvanis massif and implications for the evolution of the Eocene magmatism in the Eastern Pontides (NE Turkey). *Lithos* 125, 131–150. <https://doi.org/10.1016/j.lithos.2011.02.003>
- Vincent S.J., Allen M.B., Ismail-Zadeh A.D., Flecker R., Foland K.A. & Simmons M.D. 2005: Insights from the Talysh of Azerbaijan into the Paleogene evolution of the south Caspian region. *Geological Society of America Bulletin* 117, 1513–1533. <https://doi.org/10.1130/B25690.1>
- Wu Y.B. & Zheng Y.F. 2004: Genesis of zircon and its constraints on interpretation of U–Pb age. *Chinese Science Bulletin* 49, 1554–1569. <https://doi.org/10.1007/BF03184122>
- Yilmaz A., Adamia Sh., Chabukiani A., Chkhotua T., Erdogan K., Tuzcu S. & Karabilykoglou M. 2000: Structural correlation of the southern Transcaucasus (Georgia)–eastern Pontides (Turkey). *Geological Society London Special Publications* 173, 171–182. <https://doi.org/10.1144/GSL.SP.2000.173.01.08>
- Yilmaz Y., Tuysus O., Yigitbas E., Can Genc S. & Sengor A.M.C. 1997: Geology and tectonic evolution of the Pontides. *AAPG Memoir* 68, 183–226. <https://doi.org/10.1306/M68612C11>
- Yu K., Liu Y., Hu Q., Ducea M.N., Hu Z., Zong K. & Chen H. 2018: Magma Recharge and Reactive Bulk Assimilation in Enclave-Bearing Granitoids, Tonglu, South China. *Journal of Petrology* 59, 1–30. <https://doi.org/10.1093/petrology/egy044>
- Zakariadze S., Dilek I., Adamia S., Oberhänsli R.E., Karpemko S.F., Bazylev B.A. & Soloveva N. 2007: Geochemistry and Geochronology of the Neoproterozoic Pan-African Transcaucasian Massif (Republic of Georgia) and implication for island arc evolution of the Precambrian Arabian-Nubian Shield. *Gondwana Research* 11, 92–108. <https://doi.org/10.1016/j.gr.2006.05.012>
- Zaridze G. & Shengelia D. 1978: Hercynian magmatism and metamorphism of the Greater Caucasus in the light of plate tectonics. *Bulletin de la Societe Geologique de France* S7-XX, 355–359. <https://doi.org/10.2113/gssgfbull.S7-XX.3.355>
- Zhao K.D., Jiang S.Y., Yang S.Y., Dai B.Z. & Lu J.J. 2012: Mineral chemistry, trace elements and Sr/Nd/Hf isotope geochemistry and petrogenesis of Cailing and Furong granites and mafic enclaves from the Qitianling batholith in the Shi-Hang zone, South China. *Gondwana Research* 22, 310–324. <https://doi.org/10.1016/j.gr.2011.09.010>
- Zonenshain L.P. & Le Pichon X. 1986: Deep basins of the Black Sea and Caspian Sea as remnants of Mesozoic back-arc basins. *Tectonophysics* 123, 181–211. [https://doi.org/10.1016/0040-1951\(86\)90197-6](https://doi.org/10.1016/0040-1951(86)90197-6)